Title: Exploring the Lightning Jump Characteristics

Authors:

T. Chronis[1], L. D. Carey[1], C. J. Schultz[1,2], E. V. Schultz[1], K. M. Calhoun[3], and S. J. Goodman[4]

[1] University of Alabama in Huntsville, Earth System Science Center

[2] NASA Marshal Space Flight Center

[3] Oklahoma University Cooperative Institute of Mesoscale Meteorology Studies, National Severe Strom Laboratory,

[4] NOAA Satellite and Information Service (NESDIS)

Corresponding Author: Themis Chronis, themis.chronis@nsstc.uah.edu

University of Alabama in Huntsville

Earth System Science Center

320 Sparkman Dr., Huntsville 35805, AL

Abstract

This study is concerned with the characteristics of storms exhibiting an abrupt temporal increase in the total lightning flash rate (i.e., lightning jump, LJ). An automated storm tracking method is used to identify storm "clusters" and total lightning activity from three different lightning detection systems over Oklahoma, northern Alabama and Washington, D.C. On average and for different employed thresholds, the clusters that encompass at least one LJ (LJ1) last longer, relate to higher Maximum Expected Size of Hail, Vertical Integrated Liquid and lightning flash rates (area-normalized) than the clusters that did not exhibit any LJ (LJ0). The respective mean values for LJ1 (LJ0) clusters are 80 min (35 min), 14 mm (8 mm), 25 kg m^{-2} (18 kg m^{-2}) and 0.05 flash min^{-1} km^{-2} (0.01 flash min^{-1} km^{-2}). Furthermore, the LJ1 clusters are also characterized by slower decaying autocorrelation functions, a result that implies a less "random" behavior in the temporal flash rate evolution. In addition, the temporal occurrence of the last LJ provides an estimate of the time remaining to the storm's dissipation. Depending of the LJ strength (i.e., varying thresholds), these values typically range between 20-60 min, with stronger jumps indicating more time until storm decay. This study's results support the hypothesis that the LJ is a proxy for the storm's kinematic and microphysical state rather than a coincidental value.

1. **Introduction**

The advent of ground-based lightning detection networks in recent decades has made real-time retrieval of total lightning activity (cloud-to-ground, CG and the intracloud, IC) available in both high spatial and temporal resolutions. Although there are uncertainties in the details (Takahashi 1978; Saunders 1993), it is known that rebounding collisions between graupel and ice crystals in the presence of super-cooled water is the primary process for thunderstorm electrification (MacGorman and Morgenstern 1998; Saunders et al. 2006; Emersic and Saunders 2010). Several studies have documented a temporal co-variability between updraft mass flux, precipitation ice mass and overall storm depth with the respective total lightning activity (e.g., Goodman et al. 1988; Carey and Rutledge 2000; Chronis et al. 2007; Deierling and Petersen 2008; Bruning and MacGorman 2013). Hence, it would be reasonable to suggest that an abrupt temporal change of the order of a few minutes in the total lightning activity is considered as a severe weather indicator (“Lightning Jump", LJ, see Schultz et al. 2009; 2011). Studies by Williams et al. (1999), Gatlin and Goodman (2010), Carey et al. (2009), Schultz et. al. (2009; 2011) and Rudlosky and Fuelberg (2013) document that statistics such as lead time, probability of detection and false alarm ratio could be improved based on the use of total lightning as a metric for storm intensity. Nonetheless, these methods can be hindered by problems related to uncertainties in severe weather observations at the surface (Trapp et al. 2006; Keene et al. 2008; Schultz et al. 2011). This study puts forward an original comparison between the convective characteristics of storms that did or did not exhibit a LJ throughout their lifetime. This evaluation relies on radar-derived and lightning properties.

2. Data and Methods

2.1 Storm Tracking and Clustering

The storm identification and tracking have been performed in real-time utilizing the Warning Decision Support System Integrated Information tracking system (WDSS-II, Lakshmanan et al. 2007). A storm "cluster" is automatically identified by the reflectivity across the -10°C isothermal layer, following a merger of individual WSR-88D radars. A combination of watershed segmentation and k-means clustering is employed to identify the storm clusters (Lakshmanan et al. 2009; Kolodziej Hobson et al. 2012; Cintineo et al. 2014). To complete the storm identification, the algorithm searches for local reflectivity (Z) maxima where Z > 20 dBZ, then incrementally grows the area until it is at least 200 km^2. The storm cluster is then matched with a separately identified cluster at the next time step (for our analysis, a 1-min time step was used) using a cost function, where longer-lived cells are given preference in the case of storm mergers.

Each storm (hereinafter cluster) is described by a geolocated polygon (i.e. footprint). The cluster's lifespan is determined as the total time a cluster was identified and tracked by WDSS-II (Lakshmanan and Smith 2009). The Maximum Vertical Integrated Liquid (VIL, Greene and Clark 1972) and the Maximum Expected Size of Hail (MESH, Witt et al. 1998; Cintineo et al. 2012) are retrieved for each cluster for the duration of its lifetime. Both VIL and MESH have been used as radar-derived intensity metrics for storm properties such as liquid precipitation, updraft strength and hail growth (Amburn and Wolf 1996; Witt et al. 1998). As with any proxy, there are caveats that reflect the imperfect representations of severe weather potential and emanate from parameters unrelated to the storm dynamics (e.g. distance from the radar, tilted updrafts, storm speed etc., Stumpf et al. 2004). To mitigate these effects as much as possible, all available radars in the area are used to retrieve these proxies. Five radars over each of the three locations are employed, namely, KFDR, KTLX, KVNX, KINX, KSRX for Oklahoma, KHTX, KGWX, KBMX, KDHX, KFFC for north Alabama and KLWX, KDOX, KAKQ, KCCX, KDIX for DC (radar acronyms from https://www.ncdc.noaa.gov/nexradinv/map.jsp). The data for the present study extends from 1 April 2013 through 14 August 2013.

2.2 Total Lightning Activity and the Lightning Jump Algorithm

This study employs three total lightning detection networks: 1) the Lightning Mapping Array (LMA) networks located in central/SW Oklahoma (MacGorman et al. 2008), North Alabama (Goodman et al. 2005), and Washington D.C (Krehbiel 2008) 2) the Earth Networks Total Lightning Network (ENTLN, Liu and Heckman 2010) and 3) the National Lightning Detection Network (NLDN, Cummins et al. 1995,2005, Cummins and Murphy 2009).

The LMA networks detect the very high frequency (VHF) radiation emitted during the elemental processes that compose a lightning discharge (e.g. the initial breakdown, leader propagation and other K-processes, Uman 1987) with a location accuracy measured in tens of meters and with a time resolution of 80-100 μs (Thomas et al. 2004). The LMA detects both IC and CG flashes although the distinction can be dubious due to limitations in range. The location accuracy is also range-dependent, however it is relatively constant between ~150 km radius from the respective center (Thomas et al. 2004; Koshak et al. 2004). The following analysis relies on the total lightning flashes occurring within ~120 km of the respective LMA center (Thomas et al. 2003). Lightning flashes are retrieved from the LMAs via grouping at least 10 detected VHF radiation sources, using time and space constraints (3 km and 150 ms) between the adjoining points (McCaul et al. 2008). Only flashes that begin within the storm cluster's footprint are counted towards the total flash rate. No classification between CG and IC flashes is performed using LMA data.

The ENTLN sensors operate over a wide frequency range, spanning from 1 Hz to 12 MHz. According to Liu and Heckman (2011), electric field waveforms are used in locating as well as classifying the IC and CG flashes. Multiple strokes (or individual cloud events) are clustered into a single flash if they are within 700 ms and 10 km of the first detected stroke. A flash that contains at least one return stroke is classified as a CG flash, otherwise it is classified as an IC flash.

Since the late 1980s, the National Lightning Detection Network (NLDN, Cummins et al. 1995; 1998; 2006) has served as the source for many CG lightning-related studies over the US. The network consists of 113 sensors that combine the advantages of direction finding and time-of-arrival techniques. The NLDN CG detection efficiency ranges between 90-95% over the mid latitude continental US, with a median location error better than 500 m (Cummins and Murphy 2009; Rudlosky and Fuelberg

2010). Although the NLDN is designed to primarily detect CG flashes, it has been recently reported that IC flashes are also detected depending on the restrictions applied to the processed waveforms (peak-to-zero rise time, Murphy and Nag, 2014).

The present study employs the total flash activity (IC+CG) for all lightning detection systems. Rudlosky and Fuelberg (2013) use a similar methodology for compiling lightning and radar data. Both NLDN and ENTLN have national (US) coverage. Nevertheless, for this analysis the respective total lightning activity is computed only for the clusters that are identified over a radius around where the optimum LMA operation is ensured. Further detailed comparison (e.g., relative location accuracy and detection efficiency) between the lightning detection systems lies outside the scope of this paper. However, their employment is considered as a preliminary attempt to demonstrate results pertaining to the LJ properties from lightning detection networks of different technical specifications (e.g., detection efficiency).

The 1-min flash rate is computed by adding all the flashes occurring within the footprint of the identified cluster. The LJ is objectively identified by Schultz et al. (2009; 2011). This technique uses 14 min of the cluster's most recent flash rate history. Twelve of the 14 minutes are considered to calculate the minimum jump threshold that must be exceeded for a LJ to occur. The remaining two minutes are used to determine whether the current rate of change in the total flash rate exceeds the LJ threshold. As outlined in Schultz et al. (2009; 2011), the algorithm is a 5-step process. These steps are as follows: 1) The total flash rate (f min^{-1}) from the 14 minute period is binned into two minute segments and the total flash rate is averaged (Eqn. 1)

$$FR_{avg}(t) = \frac{FR(t)+FR(t-1)}{2} (1)$$

2) The rate of change of the total flash rate (DFRDT, f min^{-2}) is calculated by subtracting consecutive bins from each other (Eqn. 2) $\frac{d}{dt} FR_{avg}(t) = \frac{FR_{avg}(t)-FR_{avg}(t-1)}{2} = DFRFT$ (2)

This results in six DFRDT values (f min^{-2}) 3) The five earliest DFRDT values in time are used to calculate the standard deviation (σ) of the population 4) If DFRDT > α * σ and the flash rate is in greater than a given flash rate threshold (FRT) then a LJ has occurred. Note that -α- represents a multiplicative factor (i.e. dimensionless) and has no relation to the standard deviation (σ). In the original studies by Schultz et al. (2009; 2011) α and FRT were set to 2.0 and 10 f m^{-1}. Also note that α is dimensionless (i.e., f min^{-2} /f min^{-2}). Here we compute the LJ based on a variable α (0.5 - 4, step of 0.5) and FRT (5-25 f m^{-1}, step of 5 f m^{-1}). The latter is employed in order to define the LJ relative strength. For example, a weaker LJ1 would have α=1.0 and FRT=10 f m^{-1} while a stronger LJ1 would be considered as α=2.0 and a FRT=15 f m^{-1} 5) This process is repeated every two minutes as new total lightning flash rates are collected until the storm dissipates.

We note that the above implemented time-window within which the LJ is calculated is based on empirical observations of the growth and decay on the convective time scale (<10-20 minutes). Had we allowed for longer periods (e.g. 40-60 minutes) into the thunderstorm's lifetime we would likely have missed the occurrence of the first LJ and potentially severe weather occurrence. This is why we've empirically tested this algorithm with over 700 storms in multiple storm environments to help understand the variability of the algorithm (Schultz et al. 2011). The choice of the 2*σ (i.e. α=2) in Schultz et al. (2011) is simply a benchmark to which this study is not tied to.

3. Analysis and Discussion

3.1 Data and Quality control

As WDSS-II tracks clusters independently of the respective total lightning activity, the number of the identified LJ0 and LJ1 clusters is considerably different. For instance more than 2,000 clusters are classified as LJ0 at α=2.0 f m^{-2} and FRT=10 f m^{-1} whereas less than 200 are classified as LJ1 for the same α and FRT values. To ensure a comparable sample size and improve the representativeness of the data, we report on the LJ0 and LJ1 clusters that exhibit sustained total lightning activity for more than 95% during their lifespan (e.g., if a cluster is tracked for 100 minutes, the cluster must exhibit total lightning activity greater than zero for at least 95 minutes). This quality constraint (QC1) may classify a slightly different number of clusters depending on the employed lightning detection system. An additional quality constraint (QC2) is applied to the clusters that start or end at a flash rate that is notably higher than zero (set to >10 f m^{-1}). Typically, these cases represent merging or splitting clusters or clusters that entered/exited the effective radius of the LMA with high flash rates. QC2 also takes care of potential problems with MESH/VIL repetitiveness due to distance from the radar. Given that the study explores aspects such as the storm duration, the clusters that failed to conform to QC2 are omitted from the analysis. Figure 1 illustrates examples from a tracked cluster that exhibits a problematic tracking (e.g. cluster entering the area with already high flash rates, Fig. 1a), a normal tracking (i.e. comply with both QC1 and QC2, Fig. 1b), a LJ0 cluster (Fig. 1c) and a LJ1 cluster (Fig. 1d) of comparable flash rates.

All three lightning detection systems indicate that the number of LJ1 clusters decreases as the α and FRT values increase (i.e. fewer clusters at higher α and FRT values, Fig. 2b, d, and f). Unlike the LJ1, the number of tracked LJ0 clusters increases as the values of α and FRT increase (Fig. 2a, c, and e). The latter should be expected since a LJ0 at e.g. α=2.0 and FRT=10 f m^{-1} will also not exhibit LJ at higher α or FRT values.

3.2 The Autocorrelation function of LJ0 and LJ1 Flash Time Series.

Autocorrelation is an essential tool for describing the independence of sequential values in a time series. A slow (fast) decaying autocorrelation function with time (i.e. lag) indicates a consistent (random) behavior of the variable under consideration (Bowerman and O'Connell 1979). For example, a slow-decaying autocorrelation function of lightning activity time-series would signal a coherent behavior in the storm's updraft speed and volume (e.g., Schultz et. al. 2009; 2011; Schultz et al. 2014). Consequently, autocorrelation can elaborate on whether the presence of a LJ relates to a numerically random increase in the total lightning activity or points to a more persistent feature of the storm's dynamical evolution. The autocorrelation function is computed for the flash rates of LJ0 and LJ1, by introducing a time lag that ranges from 1 to +N/2 minutes, where N is the number of 1-minute intervals during which the cluster is tracked (i.e., lifespan). The lag at which the Pearson correlation is reduced below the 95% significance level denotes the "*e-folding*" time.. Figure 3 illustrates the average e-folding times for the LJ0 and LJ1 clusters for different α and FRT values. The corresponding results (Fig. 3) show longer e-folding times for the LJ1 clusters. For example, the e-folding times for the LJ1 at α=2.0 and FRT=15 f m^{-1} are computed as ~12 min for LMA, 12.7 min for the ENTLN, and 11.5 min for the NLDN. Conversely, the e-folding times for the LJ0 for the same α and FRT values are consistently less than ~4.0 min for all three lightning detection systems and any given α and FRT value. Moreover, the fact that the e-folding times for LJ1 clusters increase as both α and FRT values also increase, illustrates a key observation that emphasizes the non-redundant numerical role of both variables α and FRT in the LJ algorithmic implementation (Schultz et al. 2009; 2011).

3.3 Comparison of storm severity potential and physical characteristics between the LJ0 and LJ1 clusters.

The previous section studied the LJ0 and LJ1 clusters exclusively from the standpoint of the flash rate temporal variation. This section explores the mean values of storm attributes derived from WDSS-II. As Fig. 4 demonstrates, the LJ1 clusters exhibit a longer lifespan than the respective LJ0, and this observation is consistent throughout the three lightning detection systems and all α and FRT values. For example, for α=2.0 and FRT=15 f m^{-1}, the average lifespan is 80 min, whereas the respective LJ0 lifespan is approximately 35 min. Similar behavior is evident for the mean flash rate (normalized by the cluster's footprint area, f m^{-1} km^{-2}, Fig. 5), MESH (Fig. 6) and VIL (Fig. 7) values.

In particular, Fig. 5 indicates that on average, the LJ1 clusters exhibit ~4-5 times higher flash rates than the respective LJ0. For instance, the average LJ1 flash rates for α =2.0 and FRT=15 f m^{-1} are ~0.054 f m^{-1} km^{-2} as opposed to ~0.015 f m^{-1} km^{-2} for the LJ0, an observation that is also consistent across all networks. In turn, the MESH values for the LJ1 clusters range from ~11-18 mm whereas the LJ0 corresponding values range from ~6.5-10 mm (Fig. 6). Likewise, the mean values of VIL are ~ 18 kg m^{-2} for the LJ0 and ~25 kg m^{-2} for the respective LJ1 (Fig. 7). As also highlighted in Section 3.2, higher flash rates, larger MESH and VIL values (Figs. 5-7) are found with increasing α and FRT thresholds. One could argue that it would be expected to have higher magnitudes of weather severity proxies (e.g., MESH, VIL etc.) with higher flash rates. Nevertheless, the previous results also suggest that it is not only the flash rate (i.e., FRT) that exhibits a fundamental physical tie to storm intensity but also its temporal evolution (i.e., α). The above results are also in agreement with the findings by Rudlosky and Fuelberg (2013).

3.4 LJ strength and storm decay time

The results shown in Fig. 4 support that the LJ1 clusters with larger α and FRT relate to storms with longer durations (Fig. 4). Approaching this from a different perspective one can raise the following question: "Does the strength of the final LJ occurrence relate to the remaining lifespan of the cluster?" To address this question the time elapsed from the last LJ occurrence to the last time-step that a cluster is tracked is computed in minutes. Arguably, the results in Fig. 8 corroborate that both α and FRT play a role in the storms' remaining duration which shows to increase from around 30-35 min for LJ1 of α = 1.0 and FRT=10 f m^{-1} to over 45-60 min for higher α and/or FRT values.

4. Conclusions

The observations herein indicate that the presence of LJ has implications for the storm dynamics, intensity and evolution. The e-folding times are lower for the LJ1 clusters. For example the e-folding times for the LJ1 at α =2.0 and FRT=15 f m^{-1} are computed as ~12 min for LMA, 12.7 min for the ENTLN, and 11.5 min for the NLDN. Conversely, the e-folding times for the LJ0 for the same α and FRT values are consistently less than ~4.0 min for all three lightning detection systems. Through the enhanced updraft hypothesis, these findings indicate that the presence of a LJ signals the storm's ability to sustain convection.

The study also documents that LJ1 clusters last longer and exhibit higher flash rates (area-normalized), MESH and VIL values, further corroborating previous studies that also suggest that the temporal total lightning variability is a dependable proxy for severe weather risk assessment (Williams 2001; Schultz et al. 2009; 2011; Rudlosky and Fuelberg 2013). In addition, the MESH values for the LJ1 clusters range from ~11-18 mm whereas the LJ0 respective values range from ~6.5-10 mm (Fig. 5). The mean values of VIL are ~ 18 kg m^{-2} for the LJ0 and ~25 kg m^{-2} for the LJ1 clusters.

The results throughout this analysis consistently suggest that there is no redundancy in the role of α and FRT in the LJ numerical implementation. This is shown by the increasing magnitudes of the implicated variables (e.g. e-folding time, MESH, flash rate etc., see Fig.2-7) for LJ1 clusters increase as both α and FRT values also increase. Finally, the study offers further evidence that the presence and temporal coincidence of a LJ could be viewed as a proxy of the storm's expected dissipation. Typically, these values range between 20-60 min depending on the LJ strength with stronger jumps indicating more time until storm decay.

Ongoing efforts explore the value of the LJ as a component in the operational severe weather watch/warnings issuance (Schultz et al. 2014). The upcoming Geo-stationary Lightning Mapper (GLM) onboard the GOES-R mission (Goodman et al. 2013) will provide continuous monitoring of total lightning activity across the Western Hemisphere. GLM will provide even greater detail on the linkage between temporal lightning variability and the storm evolution over areas where currently related information, including radar, is limited or nonexistent. Importantly, GLM will provide continuous coverage of total lightning over a large domain to evaluate this study on the global scale.

Acknowledgements

We acknowledge the support by GOES-R System Program as part of the GOES-R Proving Ground and Risk Reduction programs. The first and second authors also acknowledge the support by the UAH Individual Investigator Distinguished Research awards for 2014. C. Schultz would like to acknowledge the NASA Pathways Intern Program, which provided the funding for support of this work. Lightning data were kindly provided by 1) Geoffrey Stano at the NASA-Short-term Prediction Research and Transition Center (SPoRT) 2) Earth Networks for the ENTLN data and 3) Vaisala for the NLDN data. We would also like to extend a sincere thanks to the three anonymous reviewers who helped us improve this paper.

4. **References**

Amburn, S., and P. Wolf, 1996: VIL Density as a Hail Indicator. 18th Conference on Severe Local Storms. San Francisco, CA, Amer. Meteor. Soc., 581-585.

Bowerman, B. L., and O'Connell, R. T., 1979: *Time Series and Forecasting*, Duxbury Press, North Scituate, Massachusetts.

Bruning, Eric C., Donald R. MacGorman, 2013: Theory and Observations of Controls on Lightning Flash Size Spectra. *J. Atmos. Sci.*, **70**, 4012–4029.

Carey, L. D. and S. A. Rutledge, 2000: On the relationship between precipitation and lightning in tropical island convection: A C-band polarimetric radar study. Monthly Weather Review, 128, 2687–2710.

Carey, L. D., W. A. Petersen, and C. J. Schultz, 2009: A statistical framework for the development and evaluation of a lightning jump algorithm. Preprints, Fourth Conference on the Meteorological Applications of Lightning Data, Phoenix, AZ, Amer. Meteor. Soc. d

Chronis T., Williams E, Anagnostou E., Walt Petersen, 2007: Lightning as a precursor of tropical cyclogenesis, Eos Trans. AGU, 88(40), 397, 10.1029/2007EO400001.

Cintineo, L. J., Michael J. Pavolonis, Justin M. Sieglaff, Daniel T. Lindsey, 2014: An Empirical Model for Assessing the Severe Weather Potential of Developing Convection

Cintineo, L. J., Travis M. Smith, Valliappa Lakshmanan, Harold E. Brooks, Kiel L. Ortega, 2012: An Objective High-Resolution Hail Climatology of the Contiguous United States. Wea. Forecasting, 27, 1235–1248. doi: http://dx.doi.org/10.1175/WAF-D-11-00151.1

Cummins, K. L., E. A. Bardo, W. L. Hiscox, R. B. Pyle, and A. E. Pifer, 1995: NLDN '95: A combined TOA/MDF technology upgrade of the U.S. National Lightning Detection Network, 1995: International Aerospace and Ground Conference on Lightning and Static Electricity, Williamsburg, Virginia, 26-28 Sept 1995.

Cummins, K., E. P. Krider and M. Malone, 1998: The U.S. National Detection network and applications of cloud-to-ground lightning data by electric power utilities, IEEE Trans. on Electromagnetic Compatibility, Vol. 40, no. 4.

Cummins, K. L., J. Cramer, C. Biagi, E. P. Krider, J. Jerauld, M. Uman, and V. Rakov, 2006: The U.S. National Lightning Detection Network: Post-upgrade status. Second Conference on Meteorological Applications of Lightning Data, Atlanta, Georgia, American Meteorological Society.

Cummins, K. L., and M. J. Murphy, 2009: An overview of lightning locating systems: History, techniques, and data uses, with an in-depth look at the U.S. NLDN. IEEE Trans. on Electromagnetic Compatibility, 51, 3, 499- 518.

Deierling, W., and W. A. Petersen, 2008: Total lightning activity as an indicator of updraft characteristics, J. Geophys. Res., 113, D16210, doi:10.1029/2007JD009598.

Emersic, C. and C.P.R. Saunders, 2010: Further laboratory investigations into the relative diffusional growth rate theory of thunderstorm electrification. Atmos. Res., 98, doi:10.1016/j.atmosres.2010.07.011

Gatlin, P., Goodman, S.J., 2010: A total lightning trending algorithm to identify severe thunderstorms. J. Atmos. Ocean. Technol. 27, 3–22.

Goodman, S. J., D. E. Buechler, P. D. Wright, and W. D. Rust, 1988: Lightning and precipitation history of a microburst-producing storm. Geophys. Res. Lett., 15, 1185–1188.

Goodman, S. J., R. Blakeslee, H. Christian, W. Koshak, J. Bailey, J. Hall, E. McCaul, D. Beuchler, C. Darden, J. Burks, T. Bradshaw, P. Gatlin, 2005: The North Alabama Lightning Mapping Array: Recent severe storm observations and future prospects. *Atmos. Res.*, **76**, 423-437.

Goodman S, Blakeslee R, Koshak W, Mach D, Bailey J, Buechler D, Carey L, Schultz C, Bateman M, Jr. E, et al. *The GOES-R Geostationary Lightning Mapper (GLM)*. Atmospheric Research. 2013;125-126 34-49.

Greene, D. R., and R. A. Clark, 1972: Vertically integrated liquid water- A new analysis tool. Mon. Wea. Rev., 100, 548-552

Koshak, W. J., R. J. Solakiewicz, R. J. Blakeslee, S. J. Goodman, , H. J. Christian, J. M. Hall, J. C. Bailey, E. P. Krider, M. G. Bateman, D. J. Boccippio, D. M. Mach, E. W. McCaul, M. F. Stewart, D. E. Buechler, W. A. Petersen, D. J. Cecil, 2004: North Alabama Lightning Mapping Array (LMA): VHF source retrieval algorithm and error analyses, *J. Atmos. Oceanic Technol*., 21, 543-558.

Keene, K. M., P. T. Schlatter, J. E. Hales, and H. Brooks, 2008: Evaluation of NWS watch and warning performance related to tornadic events. Preprints, 24th Conf. on Severe Local Storms, Savannah, GA, Amer. Meteor. Soc., P3.19.

Krehbiel, P. R., 2008: The DC Lightning Mapping Ar- ray. Preprints, Third Conference on Meteorological Ap- plications of Lightning Data, New Orleans, LA, USA, American Meteorological Society. 3.2.

Krehbiel, P. R., 2008: The DC Lightning Mapping Array. Preprints, Third Conf. on Meteorological Applications of Lightning Data, New Orleans, LA, Amer. Meteor. Soc., 3.2. [Available online at http://ams.confex.com/ams/pdfpapers/129095.pdf.]

Lakshmanan, V., and T. Smith, 2009: Data mining storm attributes from spatial grids. J. Atmos. Oceanic Technol., 26, 2353–2365.

Lakshmanan, V., K.Hondl, and R.Rabin, 2009: An efficient, general-purpose technique for identifying storm cells in geospatial images,' J. Ocean. Atmos. Tech., vol.26, no.3, pp.523-37.

Lakshmanan, V., T. Smith, G. J. Stumpf, and, K. Hondl, 2007: The Warning Decision Support System–Integrated Information. Wea. Forecasting, 22, 596–612.

Lang, T. J., and Rutledge, S. A., 2002: Relationships between convective storm kinematics, precipitation, and lightning. Mon. Wea. Rev., 130: 2492–2506.

Liu C., and Heckman S., 2011: Using Total Lightning Data and Cell Tracking in Severe Weather Prediction, 91st AMS meeting.

MacGorman, D. and C. D. Morgenstern, 1998: Some characteristics of cloud to ground lightning in mesoscale convective systems, J. Geophys. Res., 103, D12, 14,011-14,023.

MacGorman, D.R., Rust, W.D., Schuur, T.J., Biggerstaff, M.I., Straka, J.M., Ziegler, C.L., Mansell, E.R., Bruning, E.C., Kuhlman, K.M., Lund, N.R., Biermann, N.S., Payne, C., Carey, L.D., Krehbiel, P.R., Rison, W., Eack, K.B., Beasley, W.H., 2008. TELEX: The Thunderstorm Electrification and Lightning Experiment. Bull. Am. Meteorol. Soc. 89, 997–1013.

McCaul, E. W., J. Bailey, J. Hall, S. J. Goodman, R. Blakeslee, and D. E. Buechler, 2005: A flash clustering algorithm for North Alabama Lightning Mapping Array data. Preprints, *Conf. on Meteorological Applications of Lightning Data*, San Diego, CA, Amer. Meteor. Soc., 5.2. [Available online at http://ams.confex.com/ams/Annual2005/techprogram/paper_84373.htm].

Murphy, M. J. and A. Nag, 2014: Enhanced cloud lightning performance of the U.S. National Lightning Detection Network following the 2013 upgrade, 23rd International Lightning Detection Conference & 5th International Lightning Meteorology Conference, 18-21 March, Tucson, Arizona.

Petersen, W. A., H. J. Christian, and S. A. Rutledge, 2005: TRMM observations of the global relationship between ice water content and lightning. Geophys. Res. Lett., 32, doi: 10.1029/2005GL023236.

Scott D. Rudlosky, S D., and Henry E. Fuelberg, 2010: Pre- and Postupgrade Distributions of NLDN Reported Cloud-to-Ground Lightning Characteristics in the Contiguous United States. *Mon. Wea. Rev.*, **138**, 3623ea. Re doi: http://dx.doi.org/10.1175/2010MWR3283.1

Rudlosky, Scott D., and Henry E. Fuelberg. 2013: Documenting Storm Severity in the Mid-Atlantic Region Using Lightning and Radar Information, Monthly Weather Review 141, no. 9: 3186-3202.

Saunders, C. P. R., 1993: A Review of Thunderstorm Electrification Processes. J. Appl. Meteor., 32, 642–655.

Saunders, C. P. R., H. Bax-Norman, C. Emersic, E. E. Avila, and N. E. Castellano, 2006: Laboratory studies of the effect of cloud conditions on graupel/crystal charge transfer in thunderstorm electrification. Quart. J. Roy. Meteor. Soc., 132, 2653-2673.

Schultz, C. J. L.D. Carey, E. V. Schultz, R. J. Blakeslee and S. J. Goodman, 2014: Physical and dynamical linkages between lightning jumps and storm conceptual models. Conference Proceedings 15th International Conf. on Atmospheric Electricity. Norman, OK.

Schultz, C. J., W. A. Petersen, L. D. Carey, 2011: Lightning and Severe Weather: A Comparison between Total and Cloud-to-Ground Lightning Trends. Wea. Forecasting, 26, 744–755.

Schultz, C. J., W. A. Petersen, and L. D. Carey, 2009: Preliminary development and evaluation of lightning jump algorithms for the real-time detection of severe weather. J. Appl. Meteor. Climatol., 48, 2543–2563.

Shafer, Mark A., Donald R. MacGorman, Frederick H. Carr, 2000: Cloud-to-Ground Lightning throughout the Lifetime of a Severe Storm System in Oklahoma. Mon. Wea. Rev., 128, 1798–1816.

Stumpf, G.J., T. M. Smith and J. Hocker, 2004: New hail diagnostic parameters derived by integrating multiple radars and multiple sensors. Preprints, 22nd Conf. on Severe Local Storms, Hyannis, MA, Amer. Meteor. Soc., CD-ROM, P7.8.

Uman, 1987: The Lightning Discharge, Academic Press, pp. 183

Takahashi, T., 1978: Riming electrification as a charge generating mechanism

Thomas, R. J., P. R. Krehbiel, W. Rison, S. J. Hunyady, W. P. Winn, T. Hamlin, and J. Harlin, 2004: Accuracy of the light- ning mapping array. J. Geophys. Res., 109, D14207, doi:10.1029/ 2004JD004549.

Thomas, R., P. Krehbiel, W. Rison, J. Harlin, T. Hamlin, and N. Campbell, 2003: The LMA flash algorithm. Proc. 12th Int. Conf. on Atmospheric Electricity, Versailles, France, In- ternational Commission on Atmospheric Electricity, 655–656.

Trapp, R. J., D. M. Wheatly, N. T. Atkins, and R. W. Przybylinkski, 2006: Buyer beware: Some words of caution on the use of severe wind reports in postevent assessment and research. Wea. Forecasting, 21, 408–415.

Vonnegut, B., 1963: Some facts and speculation concerning the origin and role of thunderstorm electricity. Severe Local Storms, Meteor. Monogr., Amer. Meteor. Soc., 224–241.

water on thunderstorm charging, J. Geophys. Res., 96, 11,007–11,017, doi:10.1029/91JD00970.

Wea.Forecasting. In Press. http://journals.ametsoc.org/doi/pdf/10.1175/WAF-D-13-00113.1

Williams, E. R., 1985: Large scale charge separation in thunderclouds. J. Geophys. Res., 90, 6013–6025.

Williams, E. R., Bob Boldi, Anne Matlin, Mark Weber, Steve Hodanish, Dave Sharp, Steve Goodman, Ravi Raghavan, Dennis Buechler, 1999: The behavior of total lightning activity in severe Florida thunderstorms, Atmospheric Research, Volume 51, Issues 3–4, Pages 245-265.

Williams, E.R., 2001: The Electrification of Severe Storms, Chapter 13 in Severe Convective Storms, Ed., C.A. Doswell, III, Meteorological Monograph, Vol. 28, No. 50, 527-561.

Witt, A., M. D. Eilts, G. J. Stumpf, J. T. Johnson, E. D. Mitchell, and K. W. Thomas, 1998: An enhanced hail detection algorithm for the WSR-88D. Wea. Forecasting, 13, 286-303.

Figure Captions

Figure 1: Tracked cluster that exhibits a problematic tracking (e.g. cluster entering the area with already high flash rates, Fig.1a), a normal tracking (i.e. comply with both QC1 and QC2, Fig.1b), a LJ0 cluster (Fig.1c) and a LJ1 cluster (Fig.1d) of comparable flash rates.

Figure 2: The identified number of LJ0/LJ1 clusters as a function of FRT (x-axis, f m^{-1}) and α (y-axis,), LMA-a/b, ENTLN-c/d and NLDN-e/f

Figure 3: Mean e-folding time (min) for LJ0/LJ1, as a function of FRT (x-axis, f m^{-1}) and α (y-axis,), LMA-a/b, ENTLN-c/d and NLDN-e/f

Figure 4: Mean life-span (min) for LJ0/LJ1, as a function of FRT (x-axis, f m^{-1}) and α (y-axis,), LMA-a/b, ENTLN-c/d and NLDN-e/f

Figure 5: Mean area-normalized flash rate (f m^{-1} km^{-2}) for LJ0/LJ1, as a function of FRT (x-axis, f m^{-1}) and α (y-axis,), LMA-a/b, ENTLN-c/d and NLDN-e/f

Figure 6: Mean MESH (mm) for LJ0/LJ1, as a function of FRT (x-axis, f m^{-1}) and α (y-axis,), LMA-a/b, ENTLN-c/d and NLDN-e/f

Figure 7: Mean VIL (kg m^{-2}), for LJ0/LJ1 as a function of FRT (x-axis, f m^{-1}) and α (y-axis,), LMA-a/b, ENTLN-c/d and NLDN-e/f

Figure 8: Time elapsed until the storm dissipation for LJ1 (min) (LMA-a, ENTLN-b and NLDN-c) as a function of FRT (x-axis, f m^{-1}) and α (y-axis,).

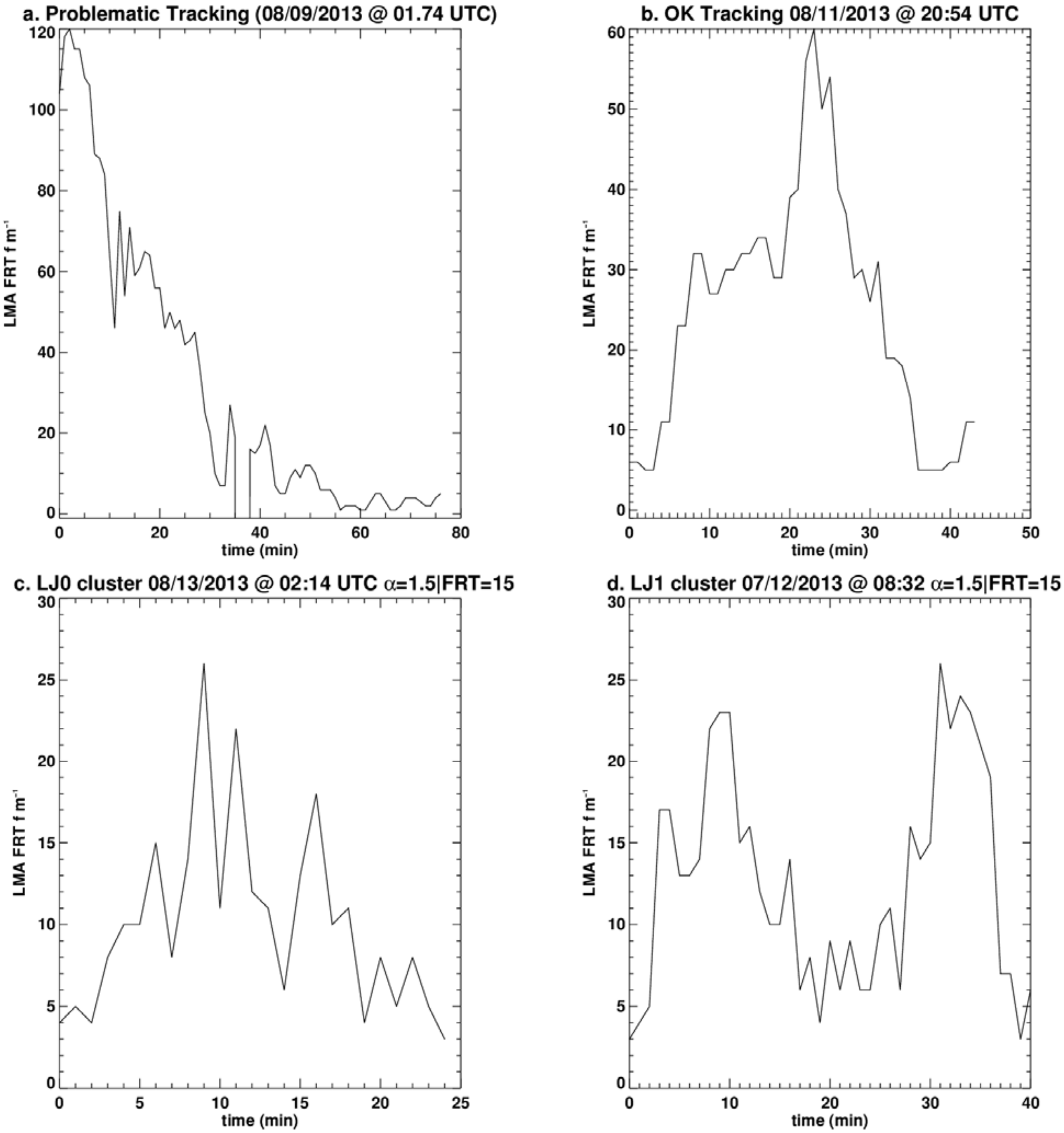

Figure 1: Tracked cluster that exhibits a problematic tracking (e.g. cluster entering the area with already high flash rates, Fig.1a), a normal tracking (i.e. comply with both QC1 and QC2, Fig.1b), a LJ0 cluster (Fig.1c) and a LJ1 cluster (Fig.1d) of comparable flash rates.

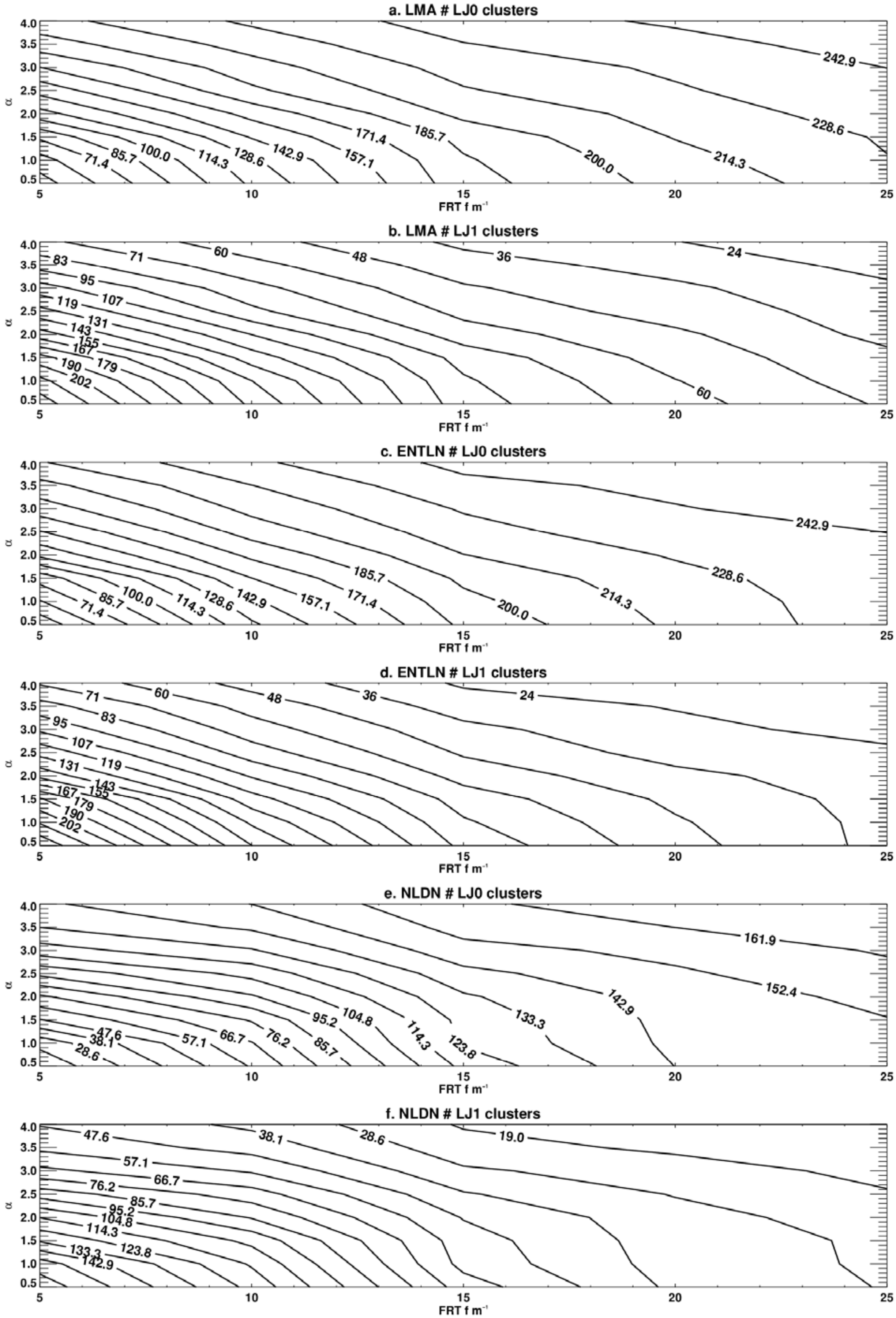
a. LMA # LJ0 clusters
b. LMA # LJ1 clusters
c. ENTLN # LJ0 clusters
d. ENTLN # LJ1 clusters
e. NLDN # LJ0 clusters
f. NLDN # LJ1 clusters
α
FRT f m⁻¹

Figure 2: The identified number of LJ0/LJ1 clusters as a function of FRT (x-axis, f m^{-1}) and α (y-axis,), LMA-a/b, ENTLN-c/d and NLDN-e/f

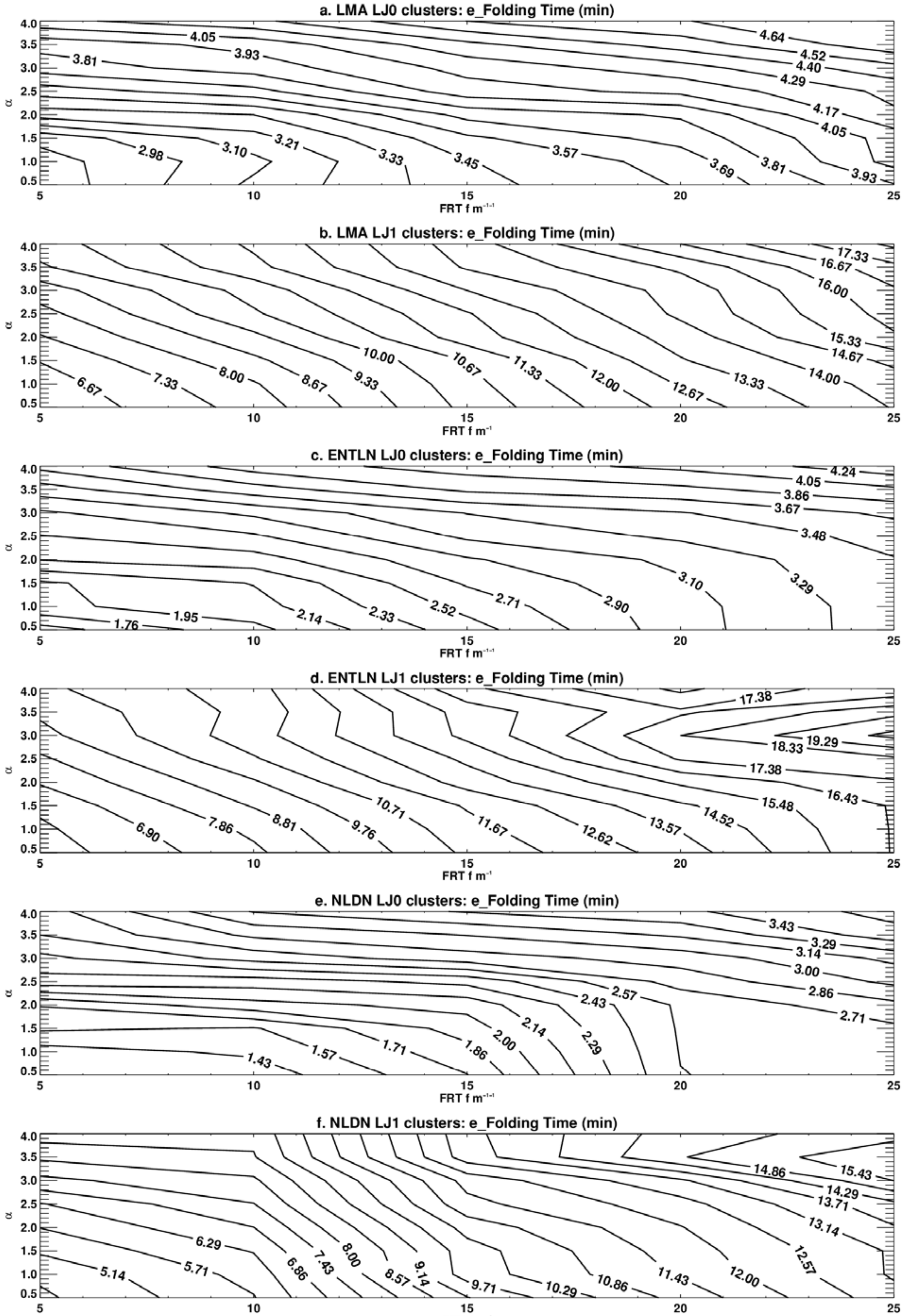
a. LMA LJ0 clusters: e_Folding Time (min)
b. LMA LJ1 clusters: e_Folding Time (min)
c. ENTLN LJ0 clusters: e_Folding Time (min)
d. ENTLN LJ1 clusters: e_Folding Time (min)
e. NLDN LJ0 clusters: e_Folding Time (min)
f. NLDN LJ1 clusters: e_Folding Time (min)
α
FRT f m⁻¹

Figure 3: Mean e-folding time (min) for LJ0/LJ1, as a function of FRT (x-axis, f m^{-1}) and α (y-axis,), LMA-a/b, ENTLN-c/d and NLDN-e/f

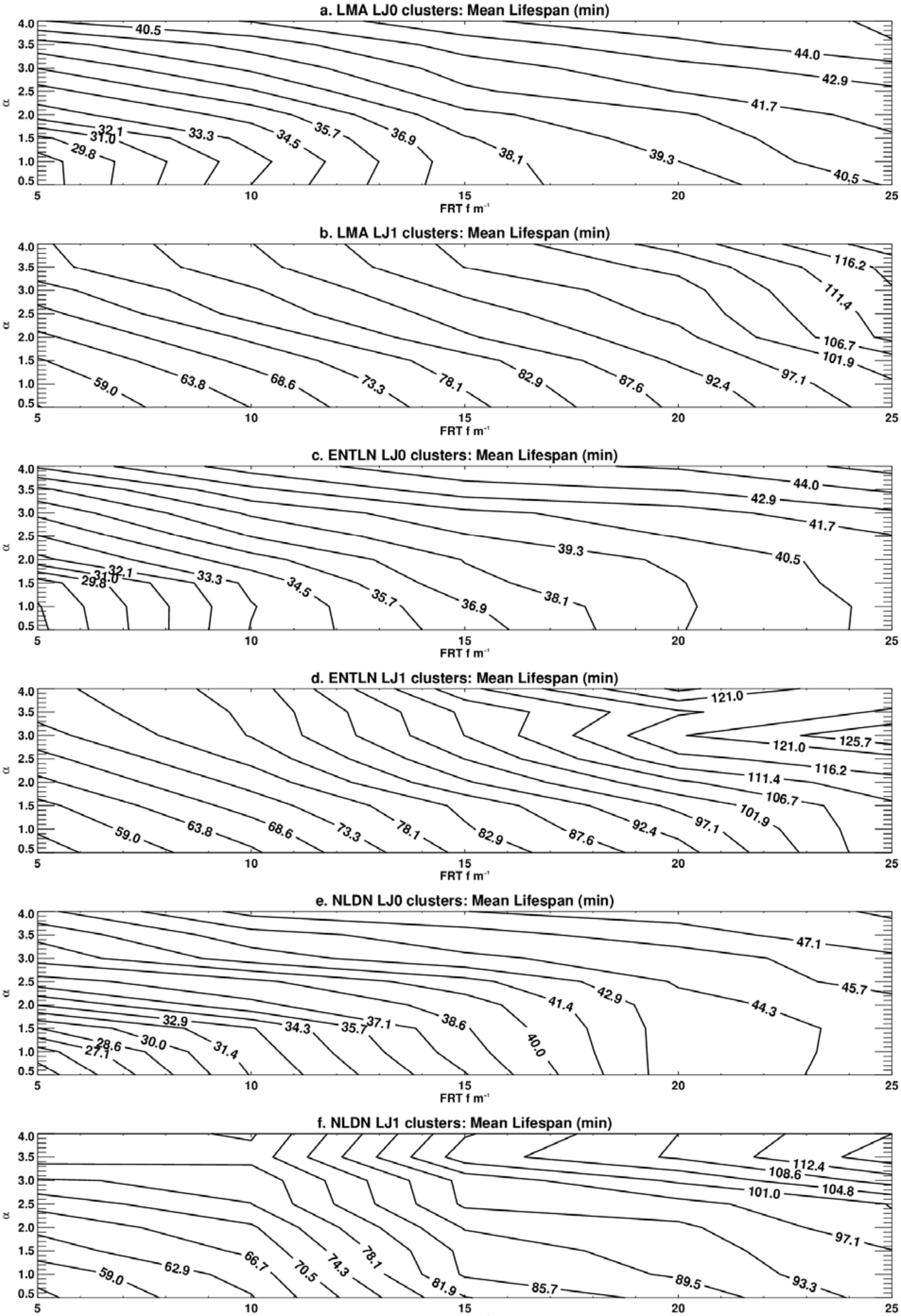
a. LMA LJ0 clusters: Mean Lifespan (min)
40.5
44.0
42.9
41.7
32.1
31.0
29.8
33.3
34.5
35.7
36.9
38.1
39.3
40.5
b. LMA LJ1 clusters: Mean Lifespan (min)
116.2
111.4
106.7
101.9
97.1
92.4
87.6
82.9
78.1
73.3
68.6
63.8
59.0
c. ENTLN LJ0 clusters: Mean Lifespan (min)
44.0
42.9
41.7
39.3
40.5
32.1
31.0
29.8
33.3
34.5
35.7
36.9
38.1
d. ENTLN LJ1 clusters: Mean Lifespan (min)
121.0
121.0
125.7
116.2
111.4
106.7
101.9
97.1
92.4
87.6
82.9
78.1
73.3
68.6
63.8
59.0
e. NLDN LJ0 clusters: Mean Lifespan (min)
47.1
45.7
44.3
42.9
41.4
40.0
38.6
37.1
35.7
34.3
32.9
31.4
30.0
28.6
27.1
f. NLDN LJ1 clusters: Mean Lifespan (min)
112.4
108.6
104.8
101.0
97.1
93.3
89.5
85.7
81.9
78.1
74.3
70.5
66.7
62.9
59.0
α
FRT f m⁻¹

Figure 4: Mean life-span (min) for LJ0/LJ1, as a function of FRT (x-axis, f m^{-1}) and α (y-axis,), LMA-a/b, ENTLN-c/d and NLDN-e/f

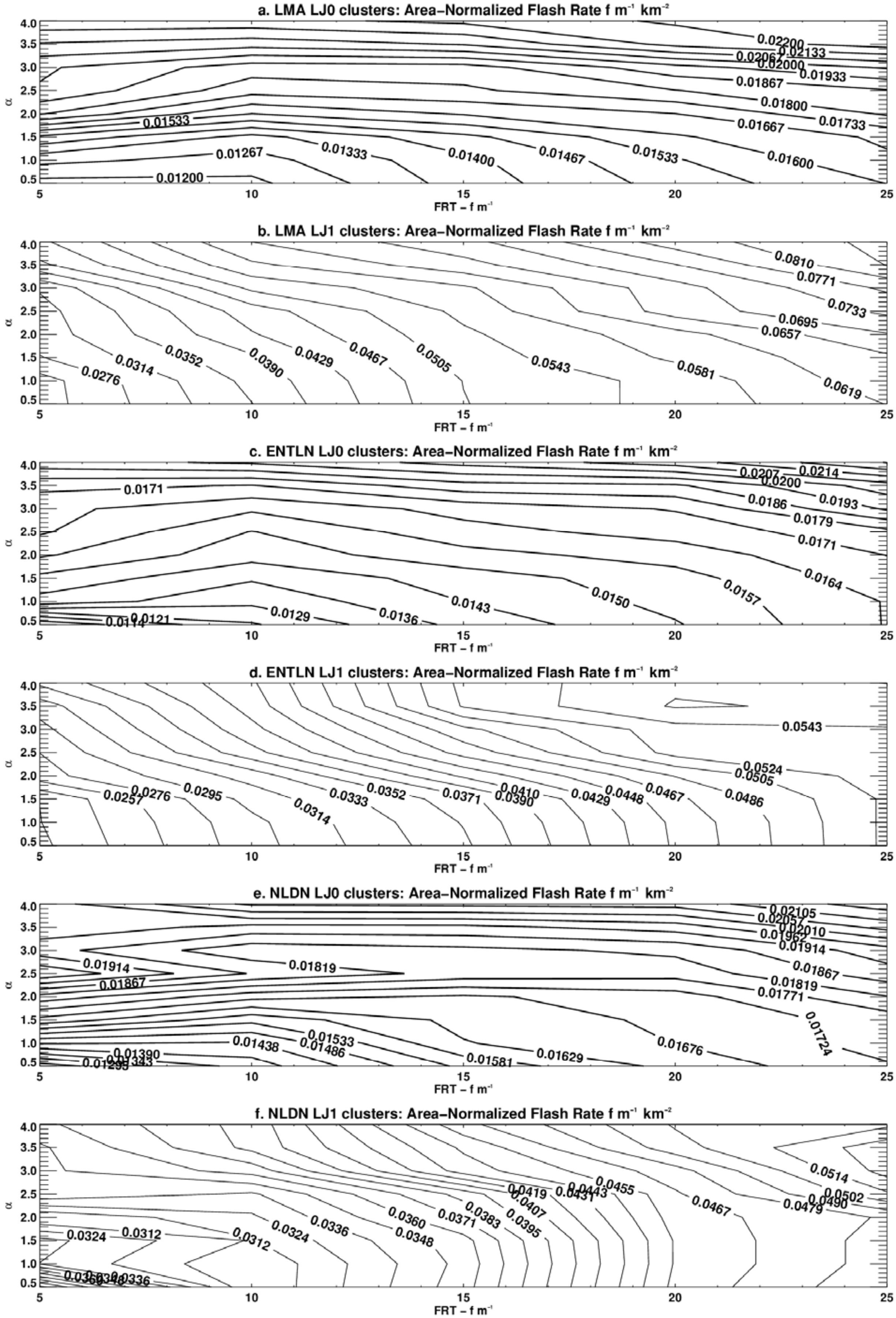
a. LMA LJ0 clusters: Area−Normalized Flash Rate f m⁻¹ km⁻²
b. LMA LJ1 clusters: Area−Normalized Flash Rate f m⁻¹ km⁻²
c. ENTLN LJ0 clusters: Area−Normalized Flash Rate f m⁻¹ km⁻²
d. ENTLN LJ1 clusters: Area−Normalized Flash Rate f m⁻¹ km⁻²
e. NLDN LJ0 clusters: Area−Normalized Flash Rate f m⁻¹ km⁻²
f. NLDN LJ1 clusters: Area−Normalized Flash Rate f m⁻¹ km⁻²
FRT − f m⁻¹
α

Figure 5: Mean area-normalized flash rate (f m^{-1} km^{-2}) for LJ0/LJ1, as a function of FRT (x-axis, f m^{-1}) and α (y-axis,), LMA-a/b, ENTLN-c/d and NLDN-e/f

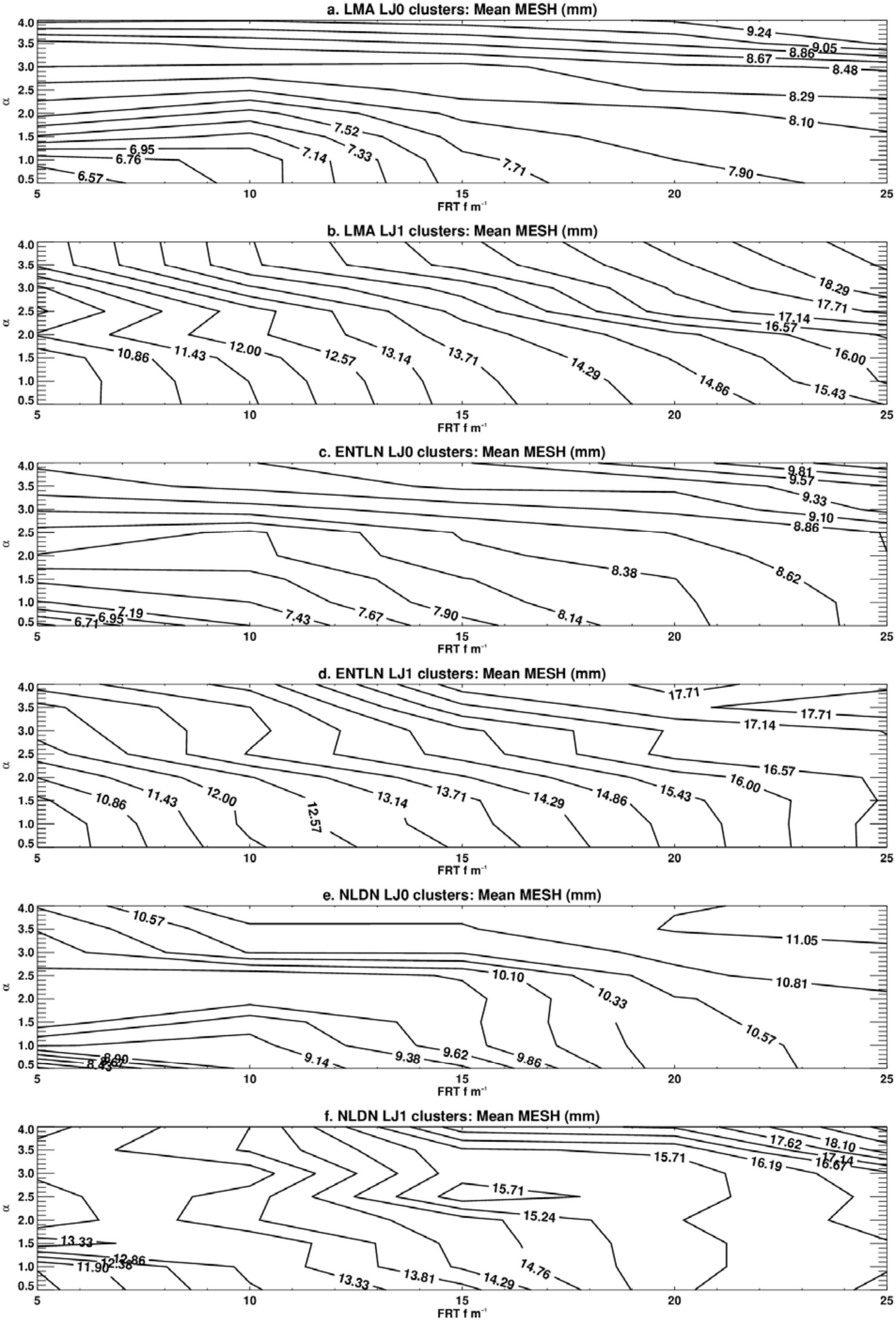
a. LMA LJ0 clusters: Mean MESH (mm)
9.24
9.05
8.86
8.67
8.48
8.29
8.10
7.90
7.71
7.52
7.33
7.14
6.95
6.76
6.57
b. LMA LJ1 clusters: Mean MESH (mm)
18.29
17.71
17.14
16.57
16.00
15.43
14.86
14.29
13.71
13.14
12.57
12.00
11.43
10.86
c. ENTLN LJ0 clusters: Mean MESH (mm)
9.81
9.57
9.33
9.10
8.86
8.62
8.38
8.14
7.90
7.67
7.43
7.19
6.95
6.71
d. ENTLN LJ1 clusters: Mean MESH (mm)
17.71
17.71
17.14
16.57
16.00
15.43
14.86
14.29
13.71
13.14
12.57
12.00
11.43
10.86
e. NLDN LJ0 clusters: Mean MESH (mm)
10.57
11.05
10.81
10.10
10.33
10.57
9.86
9.62
9.38
9.14
8.90
8.43
f. NLDN LJ1 clusters: Mean MESH (mm)
17.62
18.10
17.14
16.67
16.19
15.71
15.71
15.24
14.76
14.29
13.81
13.33
13.33
12.86
12.38
11.90
α
FRT f m⁻¹

Figure 6: Mean MESH (mm) for LJ0/LJ1, as a function of FRT (x-axis, f m^{-1}) and α (y-axis,), LMA-a/b, ENTLN-c/d and NLDN-e/f

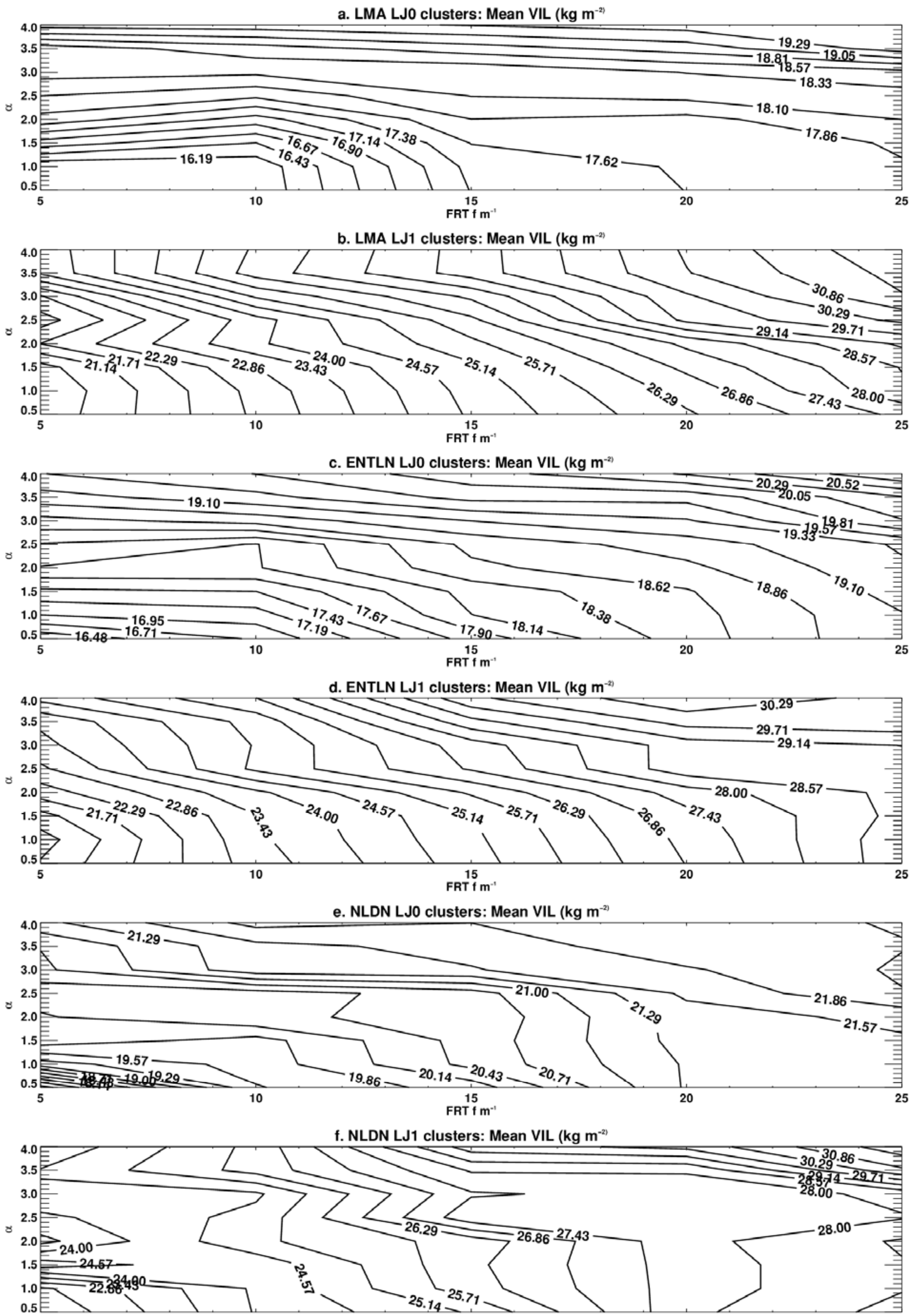
a. LMA LJ0 clusters: Mean VIL (kg m⁻²)
19.29
19.05
18.81
18.57
18.33
18.10
17.86
17.62
17.38
17.14
16.90
16.67
16.43
16.19
b. LMA LJ1 clusters: Mean VIL (kg m⁻²)
30.86
30.29
29.71
29.14
28.57
28.00
27.43
26.86
26.29
25.71
25.14
24.57
24.00
23.43
22.86
22.29
21.71
21.14
c. ENTLN LJ0 clusters: Mean VIL (kg m⁻²)
20.29
20.52
20.05
19.81
19.57
19.33
19.10
18.86
18.62
18.38
18.14
17.90
17.67
17.43
17.19
16.95
16.71
16.48
d. ENTLN LJ1 clusters: Mean VIL (kg m⁻²)
30.29
29.71
29.14
28.57
28.00
27.43
26.86
26.29
25.71
25.14
24.57
24.00
23.43
22.86
22.29
21.71
e. NLDN LJ0 clusters: Mean VIL (kg m⁻²)
21.29
21.00
21.86
21.57
20.71
20.43
20.14
19.86
19.57
19.29
19.00
f. NLDN LJ1 clusters: Mean VIL (kg m⁻²)
30.86
30.29
29.71
29.14
28.57
28.00
27.43
26.86
26.29
25.71
25.14
24.57
24.00
23.43
22.86
α
FRT f m⁻¹

Figure 7: Mean VIL (kg m^{-2}), for LJ0/LJ1 as a function of FRT (x-axis, f m^{-1}) and α (y-axis,), LMA-a/b, ENTLN-c/d and NLDN-e/f

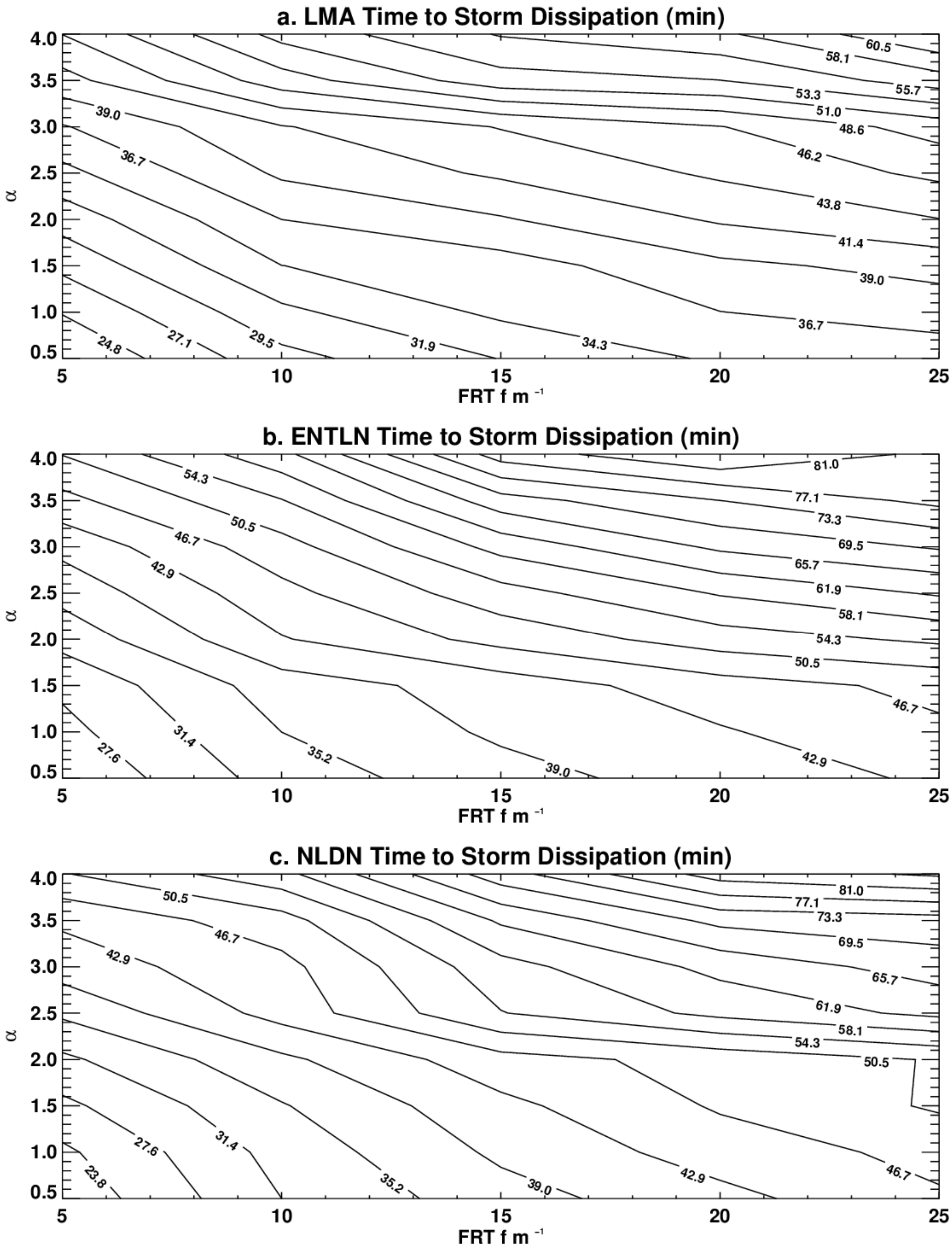
a. LMA Time to Storm Dissipation (min)
α
FRT f m ⁻¹
60.5
58.1
55.7
53.3
51.0
48.6
46.2
43.8
41.4
39.0
36.7
34.3
31.9
29.5
27.1
24.8
b. ENTLN Time to Storm Dissipation (min)
α
FRT f m ⁻¹
81.0
77.1
73.3
69.5
65.7
61.9
58.1
54.3
50.5
46.7
42.9
39.0
35.2
31.4
27.6
c. NLDN Time to Storm Dissipation (min)
α
FRT f m ⁻¹
81.0
77.1
73.3
69.5
65.7
61.9
58.1
54.3
50.5
46.7
42.9
39.0
35.2
31.4
27.6
23.8

Figure 8: Time elapsed until the storm dissipation for LJ1 (min) (LMA-a, ENTLN-b and NLDN-c) as a function of FRT (x-axis, f m^{-1}) and α (y-axis,).